IEEE Access
Multidisciplinary ⋮ Rapid Review ⋮ Open Access Journal

Received January 12, 2022, accepted February 6, 2022, date of publication February 9, 2022, date of current version February 28, 2022.

Digital Object Identifier 10.1109/ACCESS.2022.3150323

New Methodology to Calculate DC Voltage Signature in N-Phases TRUs Under Supply Voltage Sags

JAUME SAURA-PERISE, MOSTAFA BAKKAR, AND SANTIAGO BOGARRA
Department of Electrical Engineering, UPC, 08222 Terrassa, Spain

Corresponding author: Jaume Saura-Perise (jaume.saura@upc.edu)

This work was supported by the research project ''Estabilidad de redes MVDC integrando tecnologías de energías renovables, almacenamiento de energía y convertidores de fuente de impedancia,'' by the Ministerio de Ciencia, Innovación y Universidades and European Union, under Grant RTI2018-095720-B-C33.

ABSTRACT A new methodology based on the shadow projection has been developed to study any multipulse rectifier's dynamic behavior under balanced and unbalanced conditions. The proposed methodology calculates the DC average voltage and instantaneous values under balanced and unbalanced supply voltage conditions for multiphase Transformer Rectifier Units (TRUs). The calculation of the developed algorithms is more practical than the classical methods and other approaches based on Fourier series or symmetrical components that are difficult to apply under unbalanced conditions. Furthermore, classical methods are not simple to determine the limits of the integrals and calculate them to obtain the average value, so a more friendly and practical methodology has been developed to analyze rectifiers operating under supply voltage sags. This new methodology has been validated by simulation for a 12-pulse TRU in series and parallel connections, and it has also been validated for a 36-pulse TRU in parallel connection using interphase inductors. The accuracy of the calculations is validated by the experimental results for 12-pulse TRUs, series, and parallel connection, and 18-pulse TRU in series connection.

INDEX TERMS Multipulse rectifier, shadow projection, transformer rectifier unit, unbalanced voltage condition, sags.

I. INTRODUCTION

Multipulse rectifiers (MPR) have become essential in many applications such as medium-voltage variable speed drives [1] or fast-charging batteries [2], [3] to comply with the harmonic standard requirements [4]. Transformer Rectifier Units (TRUs) and Auto-Transformer Rectifier Units (ATRUs) are powered by a phase-shifting transformer with many secondary windings that depend on the number of pulses since each secondary winding feeds a six-pulse diode rectifier [5]. Other numbers of pulses can be used, such as a ten-pulse diode rectifier is applied in the case of five-phase generators [6]. The reduction of the harmonic distortion is due to the cancelation of the low-order harmonic currents generated by the rectifier [3], [7]. Moreover, multipulse rectifiers can operate at a near-unity power factor by increasing the number of pulses, and line current harmonic distortion is also reduced [8].

MPR has six-pulse diode rectifiers connected in series or parallel depending on the application. A series connection is usually used in High Voltage Direct Current (HVDC) power systems [9] and a parallel connection in electrical aircraft systems [10]. In the last century, the performance of different topologies has been presented and compared with each other [11], [12]. Some of these techniques to improve the converter systems are shown in [13]–[19]. They increase the number of pulses using different coil connection configurations. The reliability and maintenance are essential points to study in the converters to guarantee the power supply continuity [20], [21].

The dynamic behavior of a 6-pulse rectifier can be analyzed through its differential equation. As far as p-pulse rectifiers are concerned; they can also be easily studied as long as the supply voltage system is balanced because the

The associate editor coordinating the review of this manuscript and approving it for publication was Shaoyong Zheng.

commutation time instants are identical within a period, and the analytical expressions are well known [22]. However, when the supply voltage of the system is unbalanced, the analytical study gets complicated, and there are different ways in the literature to solve it. One way is to use symmetrical components and phasor approach [23], [24], while another way is to combine the Fourier's series and phasor approach [25]–[27]. In [23], a new approximated way to model unbalance voltage for ideal rectifier is shown, without AC and DC-side inductors, by introducing a deviation voltage superimposed on balanced three-phase line voltages and using symmetrical components. However, the method is only for three-phase and six-pulses, the validity of the analysis is confirmed by simulation, and no experimental results are presented. In [24], analytical expressions based on symmetrical components are used to calculate voltage and current. Moreover, the harmonics have been studied for ideal rectifiers without AC and DC-side inductors. However, the experimental results are presented only for a three-phase rectifier considering slightly unbalanced grid voltage. In [25], a systematic analytical method to calculate the harmonic components of uncontrolled single and three-phase rectifiers using Fourier series, with interphase inductors, during the continuous and discontinuous mode, has been presented. However, the analytical method is limited to single-phase and three-phase rectifiers. Also, the validity of the analysis is confirmed by simulation, and no experimental part has been presented. In [26], a fast and detailed calculation based on the Fourier series for balanced and unbalanced operation with interphase inductors has been given. Besides, the method is easy to adapt with harmonics. However, several Fourier series terms must be considered to obtain high accuracy. The validity of the analysis is confirmed by simulation, and the method is limited to a three-phase system. In [27], an average-value model of a line commutated converter-based HVDC system using Fourier series has been presented, with the advantage of lower computational requirements than a conventional electromagnetic-transient program. However, the validity of the analysis is confirmed only by simulation for a controlled twelve-pulse rectifier. In [28], the dynamic phasor model of asymmetrical 12 and 18-pulse parallel ATRU is proposed based on the switching functions expressed in the dynamic phasor domain. The presented formula calculates only the approximate value of the DC voltage, not the actual value, as not all Taylor expansion terms are used. In [29], a generalized average model is presented based on the vector concept in the *dq* frame. The model has been developed for the asymmetric 18 pulses parallel ATRUs. The developed functional models are validated through simulation and experimentally. However, a complicated process is needed to obtain the DC middle voltage.

The previous work of the author [30] is focused on the average DC voltage calculation through the perimeter of the polygon named as phasorial convex hull method, while in this paper, not only the average voltage is calculated because the instantaneous voltage is also calculated. In [30], a comparison between analytical equations and the proposed method is evaluated for ATRUs (12 and 18 pulses), and in this paper, the new method is evaluated for several TRUs (12, 18 and 36 pulses) analyzing the sag influence on the instantaneous DC voltage.

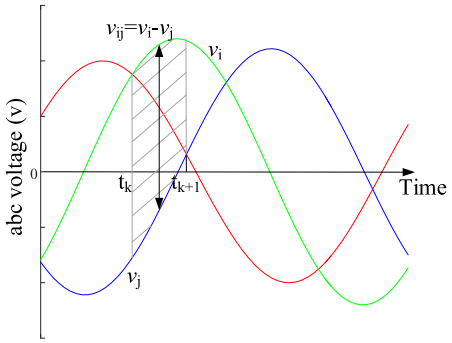

FIGURE 1. The integration limits of unbalanced supply voltages.

The present work develops a new methodology to get the output DC voltage in any *p*-pulse rectifier fed by an *N*-phase unbalanced voltage system. A simple methodology to calculate the time evolution of DC-bus voltage is given using the Shadow Projection (SP) voltage. The proposed methodology can be used for maintenance, as only the supply voltages are needed to calculate the shadow projection voltage. Measuring the DC voltage of the rectifier and comparing it with the shadow projection voltage can detect if there is a problem in the system. This problem could be orginated in the rectifier or could be an internal issue of the TRU or ATRU [21]. The method can be used to determine the elements required to reduce the effects of faults (such as voltage sags) or determine the "soft start" pre-boot elements required based on the output filter.

Furthermore, the analytical study is validated through experimental tests in the laboratory for 12 and 18-pulse rectifiers.

II. CLASSICAL MATHEMATICAL METHODS

The average value of the DC-link output voltage, V_{DC}, characterizes the behavior of the multiphase uncontrolled bridge rectifiers. This value can also be determined from the average value of the diode bridge output voltage, V_{DC}. There are different methods to calculate the voltage V_{DC}: numerical methods and analytical methods.

A. NUMERICAL METHODS

These methods use discrete values of $v_{DC}(\omega t)$ during a semi-period $T/2$ of the AC phase voltages to numerically obtain the value of V_{DC}. The main approaches are Fourier series and numerical integration. For the Fourier series, the voltage V_{DC} is obtained from the first term of the Fourier series of $v_{DC}(\omega t)$.

$$v_{DC}(\omega t) = V_{DC} + \sum_{k=1}^{\infty} V_{DCk} \cos(k\omega t + \beta_k) \qquad (1)$$

For numerical integration, the voltage V_{DC} can be numerically obtained dividing the numerical integration of $v_{DC}(\omega t)$ over a period

$$V_{\mathrm{DC}} = \frac{\Delta t}{T} \sum_{t=t_o}^{t_o+T} \frac{v_{\mathrm{DC}}(\omega(t+\Delta t)) + v_{\mathrm{DC}}(\omega t)}{2} \tag{2}$$

In unbalanced conditions, there is no expression, and then a numerical integration has to be done. V_{DC} voltage is obtained by dividing the defined integration of $v_{\mathrm{DC}}(\omega t)$, taking into account that the $v_{\mathrm{DC}}(\omega t)$ is a continuous function and in intervals corresponds to all possible phase-to-phase voltages in one period [0 $\sim$ T], as shown in Fig. 1. The difficulty arises in determining the intersections (t_{k}, $t_{\mathrm{k+1}}$) to identify each interval's integration limits, as shown in Fig. 1. By determining each interval [t_{k}, $t_{\mathrm{k+1}}$] (corresponding to each pulse), the equivalent expression of $v_{\mathrm{DC}}(\omega t)$ is determined depending on the input voltages of the rectifier.

$$V_{DC} = \frac{1}{T} \int_{t=0}^{T} v_{DC}(\omega t)dt = \frac{1}{T} \sum_{k=0}^{N_{bp}} \left(\int_{t=t_k}^{t_{k+1}} v_{ij}(\omega t)dt \right), \tag{3}$$

However, when the change of the voltage or the phase (or both) is unknown, as seen in Fig. 1, then (3) is one of the few numerical expressions that can calculate the average V_{DC} accurately, but it requires a lot of computing power.

It should be noted that, for the numerical methods, in order to have more accurate results, the calculation of the average V_{DC} voltage strongly depends on the discretization of the $v_{\mathrm{DC}}(\omega t)$.

On the other hand, numerical methods for unbalanced cases require more computing power that will increase with the number of phases of the rectifier, mainly because many definite integration intervals must be calculated.

B. ANALYTICAL METHODS

These methods are helpful to have closed-form analytical expressions for determining V_{DC} as a function of the rectifier variables to investigate their influence further. In general, Continuous Conduction Mode (CCM) is considered, and voltage drops in the AC line inductors are neglected, which allows the expression for V_{DC} calculation to be obtained from the AC phase voltages.

The analytical formula is a well-known expression for the calculation of V_{DC} in multiphase uncontrolled bridge rectifiers, which are fed by AC phase balanced sinusoidal voltages,

$$V_{\mathrm{DC}} = 2\frac{N\widehat{V}_{\mathrm{s}}}{\pi} \sin(\frac{\pi}{N}) \tag{4}$$

where $\widehat{V}_{\mathrm{s}} = \sqrt{2}V_{\mathrm{s}}$ is the peak value of the AC phase balanced sinusoidal source voltages (V_{s}), and N is the number of phases of the rectifier.

Each configuration has a specific equation for balanced and symmetrical conditions. Some of the most typical are shown in the following equations. In the case of three-phase systems, $N = 3$ phases and $V_{\mathrm{L}} = \sqrt{3}V_{\mathrm{s}}$:

$$V_{\mathrm{DC}} = 2\sqrt{2}\frac{3V_{\mathrm{L}}}{\sqrt{3}\pi} \sin(\frac{\pi}{3}) = 1.35V_{\mathrm{L}} \tag{5}$$

This is the most commonly used expression for three-phase and balanced systems where V_{L} is the RMS value of line voltage.

In the case of 12-pulse ATRU with parallel interphase inductors connection, the average DC voltage equals:

$$V_{\mathrm{DC}} = 2\frac{3\sqrt{2}V_{\mathrm{s}}/\cos(15^\circ)}{\pi} \sin\left(\frac{\pi}{3}\right) = 2.42V_{\mathrm{s}}. \tag{6}$$

In the case of the asymmetric 18-pulse delta-type ATRU described in [28], the average voltage can be determined by applying the following formula:

$$V_{\mathrm{DC}} = \sqrt{6}V_{\mathrm{s}}\frac{\sin(\pi/18)}{\pi/18} = 2.437V_{\mathrm{s}}. \tag{7}$$

It is clear that the calculation of the average V_{DC} voltage is much easier with equations (4) or (5), but it is only possible in balanced cases (amplitudes and phases). Previous equations are some examples, but for other configurations, an analytical equation can be obtained for each of them operating only in balanced conditions.

III. SHADOW PROJECTION PROPOSED METHODOLOGY

The shadow projection method is a new concept that accurately predicts the output voltage of the bridge rectifier; that is, the voltage at the input of the filter, the shadow projection is based on the frequency domain. In addition, in order to calculate the average value, it is not necessary to calculate the integrals and the corresponding integration limits. A similar idea is used in image processing to determine the bone image in 2-D or 3-D, but in reverse, the projection is determined through a known polygon. Both shadow projection and image processing are based on the Cauchy formula.

A. SHADOW PROJECION VOLTAGE SIGNATURE

Fig. 2 shows N-sources in star configuration connected to the bridge rectifier. The N-phases system is represented using a phasor system.

The voltage phasors are ordered by the value of the angle from the minimum to the maximum.

$$\varphi_1 < \ldots. < \varphi_i < \ldots. < \varphi_n$$
$$\underset{\rightarrow i}{V} = \left|\widehat{V}_i\right|_{\varphi_i},$$

where $\widehat{V}_i$ is the maximum value of the i-phase,

An imaginary polygon is constructed by the ends of two consecutive voltage vectors, as seen in Fig. 3, and every side of the polygon are defined by (L_{i}),

$$\underset{\rightarrow i}{L} = \underset{\rightarrow i+1}{V} - \underset{\rightarrow i}{V} \tag{8}$$

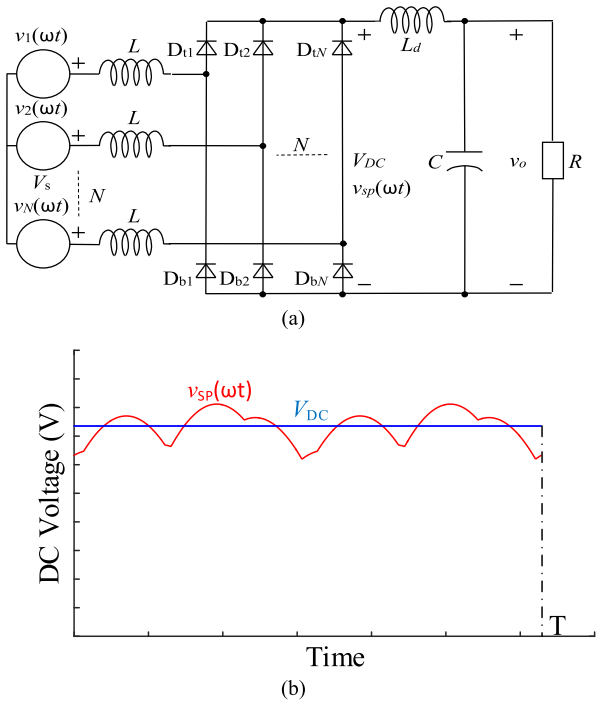

FIGURE 2. (a) Bridge rectifier with N phases, with L-C filter and a load, (b) signature of the rectifier voltage $v_{SP}(\omega t)$, and the average value V_{DC}.

which can be defined by a magnitude and an angle as follows:

$$\underset{\rightarrow i}{L} = \left|\underset{\rightarrow i}{L}\right|_{\lambda_i} \tag{9}$$

The interval t_k and t_{k+1} must be identified by the instant when the side of the phasor representing the composite voltage is perpendicular to the straight line, as seen in Fig. 3. Using this concept, (10) is obtained, and thus the time of commutation change is determined. As it is shown in Fig. 1, t_k is the end of the pulse (k) and the start of the new pulse (k + 1), and N_p is the number of pulses in a period (T), as presented by the following equation:

$$t_k = \begin{cases} 0 & k = 0 \\ \dfrac{1}{\omega}\tan^{-1}\left(\dfrac{V_i\cos(\varphi_i) - V_j\cos(\varphi_j)}{V_i\sin(\varphi_i) - V_j\sin(\varphi_j)}\right) & 1 \le k \le N_p \\ T & k = N_p + 1. \end{cases} \tag{10}$$

The shadow projection is based on the projection of all the sides of the polygon on the straight line. The straight line can be defined with a unitary vector as:

$$\underset{\rightarrow}{\alpha} = 1_{\theta-\omega t} = e^{j(\theta-\omega t)} \tag{11}$$

Usually, the initial angle of the straight line is $\theta = 0°$. As shown in Fig. 3, a cinematic graph has been presented. Due to the closed polygon, the addition of the side vectors equals zero, as seen in (12).

$$\sum_{i=1}^{n} \underset{\rightarrow i}{L} = 0 \tag{12}$$

The straight line divides the polygon into two sides (projection up (black color in Fig. 3) and projection down (orange color in Fig. 3)). The following scalar product defines the projections on the straight line for every side of the polygon

$$\left\langle \alpha, \underset{\rightarrow i}{L} \right\rangle = \overline{p_i p_{i+1}} = |\alpha| \left|\underset{\rightarrow i}{L}\right| \cos(\theta - \omega t - \lambda_i) \tag{13}$$

where $|\alpha| = 1$ at every projection depends on ωt.

The upper projection of the polygon on the straight line is in one way, and the down projection of the polygon is on the opposite way, but the absolute values of both projections are equal, as shown in Fig. 3 and (14).

$$\{|\overline{p_1p_2} + \overline{p_2p_3}|\}_{\text{up}} = \{|\overline{p_3p_4} + \overline{p_4p_5} + \overline{p_5p_1}|\}_{\text{down}} \tag{14}$$

All the polygon vertex points must be in the inferior and superior positions during one period (one turn). If not, the phase voltage that defines this vertex is not considered because the polygon is not convex, as shown in Fig. 4. This idea is used to define the polygon, which must be convex. If the absolute values of the up and down projections are added, all the projections are included twice.

$$\left\{\left|\overline{\mathrm{P}_{rojection}}\right|\right\}_{\text{up}} + \left\{\left|\overline{\mathrm{P}_{rojection}}\right|\right\}_{\text{down}} = \sum_{i=1}^{n} |\overline{p_i p_{i+1}}| \tag{15}$$

As the up and down projection are the same, then only one projection is needed, therefore:

$$\left\{\left|\overline{\mathrm{P}_{rojection}}\right|\right\} = \frac{\sum_{i=1}^{n} \overline{|p_i p_{i+1}|}}{2} \tag{16}$$

The advantage of (16) is that it is not required to identify the limits calculated using (10), saving the computation time. The projection is the actual instantaneous value of $v_{SP}(\omega t)$, then the shadow projection methodology is represented by (17), with that the numerical process is determined the DC voltage signature in a period. As shown in Fig. 2, $v_{SP}(\omega t)$ is the voltage at the output of the rectifier and before the filter, in CCM.

$$v_{SP}(\omega t) = \frac{\sum_{i=1}^{n} |\overline{p_i p_{i+1}}|}{2} = \frac{\sum_{i=1}^{n} \left|\underset{\rightarrow i}{L}\right| |\cos(\theta - \omega t - \lambda_i)|}{2}$$
$$v_{SP}(\omega t) = \frac{\sum_{i=1}^{n} \left|Re\left(\underset{\rightarrow i}{L}\,\underset{\rightarrow}{\alpha}\right)\right|}{2} \tag{17}$$

B. AVERAGE VALUE CALCULATION

Another way to demonstrate the average value different from [30], which is based on the Phasorial convex hull method, is presented in this section. In order to know the average projection of the polygon, first, the average projection of one side of the polygon needs to be calculated. The upper and lower limits of the integration need to be identified for every projection. Every side of the polygon starts the projection when it is perpendicular to the straight

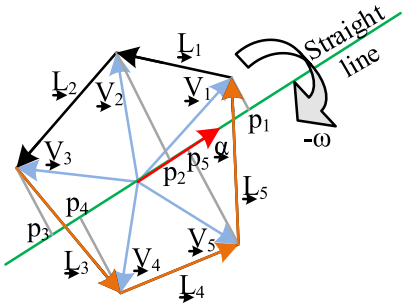

FIGURE 3. A convex polygon defined by phase voltages and a straight line rotating in clockwise.

line in the inferior position of the straight line and finish after a π radians when the side vector is again perpendicular in the opposite way on the upper position of the straight line, that means the side voltage vector is at 90° from the straight line in the inferior position, and at −90° in the superior position. These limits are based on this idea and calculated using:

$$\theta - \omega t_{i\,\mathrm{inf}} - \lambda_i = -\frac{\pi}{2}, \quad \theta - \omega t_{i\,\mathrm{sup}} - \lambda_i = \frac{\pi}{2} \tag{18}$$

The average projection per turn of the segment equals the average value.

$$\begin{aligned}\overline{\overline{p_i p_{i+1}}} &= \frac{1}{\pi}\int_{\omega t_{\mathrm{inf}}}^{\omega t_{\mathrm{sup}}} \overline{p_i p_{i+1}}\, d\omega t \\ &= \frac{1}{\pi}\int_{\theta-\lambda_i+\frac{\pi}{2}}^{\theta-\lambda_i-\frac{\pi}{2}} \left|\underset{\rightarrow i}{L}\right| * \cos\left(\theta - \omega t - \lambda_i\right) d\omega t\end{aligned} \tag{19}$$

The solution of the definite integral is:

$$\overline{\overline{p_i p_{i+1}}} = \frac{1}{\pi}\left|\underset{\rightarrow i}{L}\right| \left(\sin(\frac{\pi}{2}) - \sin(-\frac{\pi}{2})\right) \tag{20}$$

By operating and simplifying, the following equation is obtained:

$$\overline{\overline{p_i p_{i+1}}} = \frac{2\left|\underset{\rightarrow i}{L}\right|}{\pi} \tag{21}$$

The average projection of the polygon is the addition of all the average projections of every side divided by two:

$$V_{\mathrm{DC}} = \frac{\sum_{i=1}^{n} \overline{\overline{p_i p_{i+1}}}}{2} = \sum_{i=1}^{n} \frac{2\left|\underset{\rightarrow i}{L}\right|}{2\pi} = \frac{\text{Polygon perimeter}}{\pi} \tag{22}$$

The following conclusions are summarized:

- The perimeter of a polygon divided by π is equal to the average projection of the polygon over the straight line.
- Any non-convex polygon can be transformed to a convex one, removing the non-convex (vertex) ends by connecting the two consecutive convex (vertex) ends, forming a new side, and eliminating the concave sides. In this case, the polygon will be losing one side, as shown in Fig. 4.
- If the system is single-phase or two-phases, it can be considered as a rectangle of zero width, consisting of two faces, thus

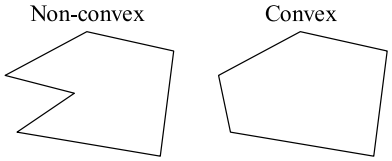

FIGURE 4. Conversion of non-convex to convex polygon.

$$V_{DC} = \frac{|V_{AN}| + |V_{NA}|}{\pi} \quad V_{DC} = \frac{|V_{AB}| + |V_{BA}|}{\pi} \tag{23}$$

- Only (22) is needed to calculate the average value for different configurations.
- The shadow projection method is ideal for calculating the DC voltage. The voltage drop can be introduced to calculate the actual values, as follows

$$V_{\mathrm{DC\ real}} = V_{\mathrm{DC\ composed}} - \sum V_{\mathrm{drop}} \tag{24}$$

Usually, the voltage drop is represented with an equivalent resistor and an equivalent inductor, as in (25),

$$V_{\mathrm{DC\ real}} = V_{\mathrm{SP}} - R_{\mathrm{eq}} \cdot i_{\mathrm{DC}} - L_{\mathrm{eq}} \frac{di_{DC}}{dt} \tag{25}$$

There are different ways to connect the rectifiers, series, parallel, and adding interphase inductors. In these cases, the shadow projection comprises the formulas (26) for series connection and (27) for parallel connection.

$$v_{\mathrm{DC\ composed\_S}}(\omega t) = \sum_{i=1}^{n_s} v_{\mathrm{SP}i}(\omega t). \tag{26}$$

$$v_{\mathrm{DC\ composed\_P}}(\omega t) = \max\left(v_{\mathrm{SP1}}(\omega t), \ldots . v_{\mathrm{SPn_p}}(\omega t)\right) \tag{27}$$

When n rectifiers are connected in parallel, and interphase inductors are used, the DC voltage ($v_{\mathrm{DC\ composed\_L}}$) can be calculated using the following equation:

$$v_{\mathrm{DC\ composed\_L}}(\omega t) = \sum_{i=1}^{n_s} \frac{v_{\mathrm{SP}i}(\omega t)}{n}. \tag{28}$$

Table 1 compares the shadow projection methodology and classical methods, and the advantages of the shadow projection are highlighted.

IV. SHADOW PROJECTION METHODOLOGY APPLIED TO TRUs UNDER SUPPLY VOLTAGE SAGS

This section will apply the shadow projection method for different TRUs in series and parallel connections under supply voltage sags.

A. GENERAL METHOD

Three-phase systems have been extensively studied; however, nowadays, more applications require a more secure supply and torque as military applications, ships, airplanes, and wind generators.

This section presents an example of a six-phase system to explain the proposed method, as shown in Fig. 5, where a sag occurs in phase "*e*". Fig. 5(a) shows the classical method to determine the average voltage for multiphase systems in

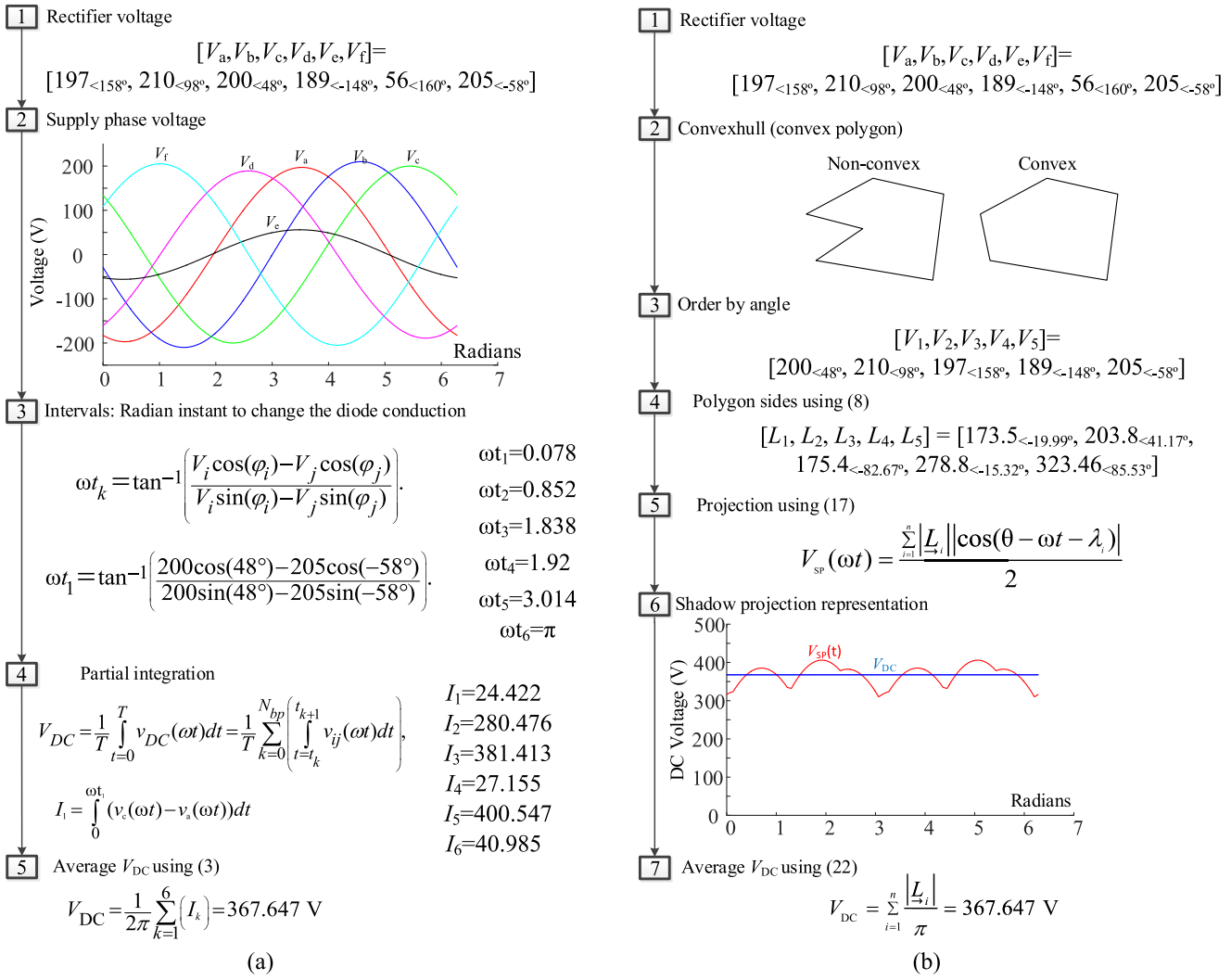

FIGURE 5. The flowchart of a general process to obtain the shadow projection voltage (a) classic process, (b) shadow projection process.

unbalanced conditions. First, the supply phases are presented, and as seen, the V_e does not be considered because its value is less than the values of other phases. Then equation (10) is used to calculate the instant when begins the new interval. The integration limits are the beginning and the end of the interval. The maximum and minimum voltages in each interval have to be determined, and then their difference is the instantaneous DC voltage in each interval ($v_{ij} = v_i$-v_j), as seen in Fig. 1. Finally, all the partial integrations of the DC voltage are added and divided by the period to calculate the average DC value. As seen, the method is complicated and needs many steps to obtain the average DC value.

In Fig. 5(b), the shadow projection method is shown. Firstly, the supply phases are presented. Secondly, the convex hull function is applied, then the non-convex phases are eliminated. In this case, as the initial polygon is not convex, the V_e voltage is discarded, and the rest of the voltages are ordered by their angle. In the next step, the sides of the convex polygon are calculated. The addition of all the sides calculates the perimeter of the convex polygon and then is divided by π; this value equals the average value, as shown in (22).

In Fig. 5(b), the instantaneous value is also calculated using shadow projection methodology. First, the projection of every side of the polygon to the straight line is calculated. Finally, the instantaneous value is obtained by adding all of them and dividing them by two, as shown in (17). The previous step is performed in every instant to construct the signature. In (17), only ωt is changing, and the rest of the parameters are constant.

B. 12-PULSES TRUs SERIES AND PARALLEL CONNECTION

The systems in Fig. 6 have been studied during a sag. The connection of the transformer Dy11d0 is shown in Fig. 6, in series and parallel connections. In this case, there are three phases connected to each rectifier at the secondary of the transformer, which means there are two polygons, one for every rectifier. The two polygons are shown in Fig. 7, and the projection to the straight line can be observed in Fig. 8 when they are positioned in the same center of rotation.

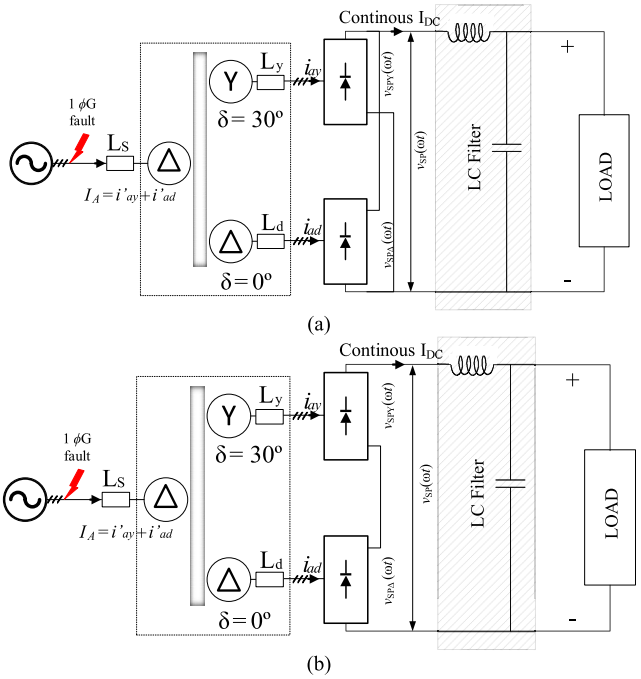

FIGURE 6. Dy11d0 transformer with 12 pulses bridge connections (a) parallel, (b) series.

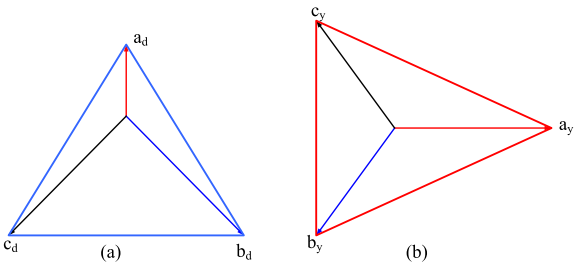

FIGURE 7. Delta-star polygon connection at the secondary of the transformer Dy11d0 after a sag type B, and $h = 0.3$ (a) delta connection, (b) star connection.

The system has been tested in the lab, but previously, in order to understand how to apply the shadow projectcion methodology, it is considered a 15 kV voltage applied to the primary (in the second step of Fig. 9), and then 400 V are available in the secondaries (in the third step of Fig. 9). A sag type B was applied to the supply voltage, with $h = 0.3$ for parallel and series connections, the parameter h is related to the sag depth, defined according to Table 1 from [31], as follows for type B sag.

$$V_A = h^* V, \quad V_B = -V(\frac{1}{2} + j\frac{\sqrt{3}}{2}), \quad V_C = -V(\frac{1}{2} - j\frac{\sqrt{3}}{2}) \tag{29}$$

In the fourth step of Fig. 9, the shadow projection is calculated for star and delta connections, and the signature depends on the degree shifting of the transformer. These projections are equivalent to the instant voltage on every rectifier, the blue projection to the rectifier connected to the delta, and the red projection to the rectifier connected to the star (Fig. 8). In serial connection (26), both projections are added, but in parallel connection (27), only the maximum value must be considered. The instantaneous $v_{SP}(\omega t)$, shown in Fig. 9 (steps 5 and 6), is represented in green, the projection from the output of the rectifier connected to the Y secondary is in red, and the corresponding to the Δ secondary is in blue. The same system considering ideal diodes has been simulated in MATLAB™, and the results match perfectly.

This system has been implemented in the lab using a 4 kVA, 400/230/230 V transformer, and in Fig. 10, the experimental results are compared with the results obtained using the shadow projection methodology for parallel and series connections.

Fig. 10 (a) shows how the experimentally signature corresponds to the green signature obtained in step 5 of

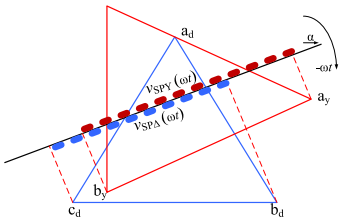

FIGURE 8. Polygon of delta and star bridges, the straight line and the instant value of shadow projection.

TABLE 1. Comparison between classical process and shadow projection.

	Classical process	Shadow projection
advantages	- Easier concept - Easier in case of three phase balanced process	- Faster - Less power calculation - Easier application for multi-phases and unbalanced process - Average and instantaneous values are obtained
disadvantages	- Complicated calculation with arctan and integral - Longer process with many intervals - Not possible to calculate the instantaneous value - Very complicated in case of multi-phases and unbalanced process	- Understanding the new methodology

TABLE 2. Conduction intervals during a sag in parallel connection.

Intervals	Limits
Int. 1	$0.00 < \omega t < 0.42$
Int. 2	$0.42 < \omega t < 1.03$
Int. 3	$1.03 < \omega t < 1.41$
Int. 4	$1.41 < \omega t < 1.73$
Int. 5	$1.73 < \omega t < 2.11$
Int. 6	$2.11 < \omega t < 2.72$
Int. 7	$2.72 < \omega t < 0.42+\pi$
Int. 8	$0.42+\pi < \omega t < 1.03+\pi$
Int. 9	$1.03+\pi < \omega t < 1.41+\pi$
Int. 10	$1.41+\pi < \omega t < 1.73+\pi$
Int. 11	$1.73+\pi < \omega t < 2.11+\pi$
Int. 12	$2.11+\pi < \omega t < 2.72+\pi$

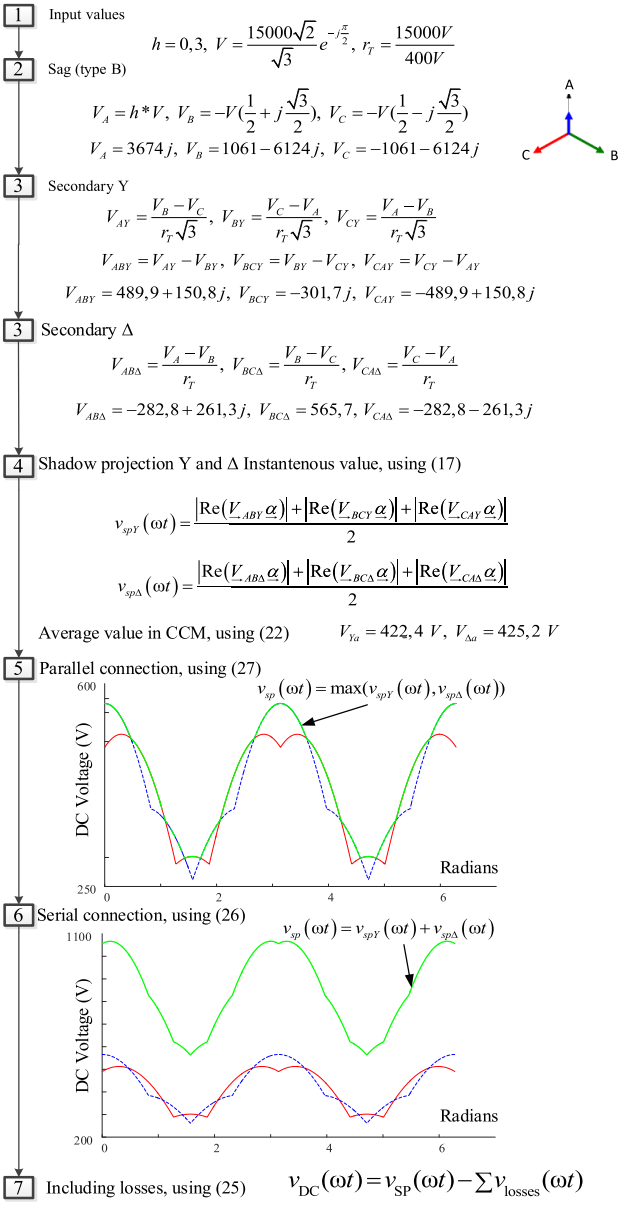

FIGURE 9. Flowchart of 12 pulse rectifier during unbalanced process to obtain the shadow projection voltage.

Fig. 9, calculated as the maximum value of the two voltages projected by the Star and triangle rectifier. It can also be observed that the inflection points correspond to the points where the projected voltages v_{SPY} (ωt) and v_{SPD} (ωt) are intersected, but do not correspond to the change in normal conduction of the diodes of one rectifier, because at each time only one rectifier is operating.

Fig. 10 (b) shows how the experimentally signature corresponds to the green signature obtained in step 6 of Fig. 9, calculated as the sum of the two voltages projected by the Star rectifier and the Triangle rectifier. It is also observed that the changes of inflection points being the sum are the moments of change of normal conduction of direct and inverse diodes in both rectifiers.

TABLE 3. Conduction intervals during a sag in series connection.

Intervals	Limits
Int. 1	$0.00 < \omega t < 0.766$
Int. 2	$0.766 < \omega t < 1.237$
Int. 3	$1.237 < \omega t < \pi/2$
Int. 4	$\pi/2 < \omega t < 1.904$
Int. 5	$1.904 < \omega t < 2.375$
Int. 6	$2.375 < \omega t < \pi$
Int. 7	$\pi < \omega t < 0.766 + \pi$
Int. 8	$0.766 + \pi < \omega t < 1.237 + \pi$
Int. 9	$1.237 + \pi < \omega t < 3\pi/2$
Int. 10	$3\pi/2 < \omega t < 1.904 + \pi$
Int. 11	$1.904 + \pi < \omega t < 2.375 + \pi$
Int. 12	$2.375 + \pi < \omega t < 2\pi$

In Table 2, the limits of integration are presented for the parallel connection used in the classic model, representing the change of diode conduction (10). Also, in Table 3, the limits of integration are presented for the series connection. In Table 2 and Table 3, only one period is represented, but other periods can be represented by adding n*ωT, where n is the number of the period, ω is the pulsation, and T is the period. The values of the Table 3 are calculated using equation (10) to localize the intervals, taking into account that in a series connection, the commutation instant in the 12 pulses case is composed adding the 6-pulse commutations of star and delta. As shown in the right part of Fig. 10, the notch in the 12 pulses case is lower than in the six pulses case because the voltage difference is reduced due to the increase in the number of pulses.

In every studied case, the shadow projection can be calculated for the half period because the other half is the same. For the experimental results, the notch has a delay, as seen in Fig. 10, from the calculated results, because a voltage difference is required to do the commutation.

The output 12-pulse TRU obtained experimentally for parallel connection agrees with the maximum instantaneous voltages from star or delta connections obtained in (30).

$$v_{sp}\,(wt) = \max(v_{spY}\,(wt)\,, v_{sp\Delta}\,(wt)) \tag{30}$$

The output 12-pulse TRU obtained experimentally for serial connection agrees with the addition of the instantaneous voltages from the star and delta connections obtained in (31).

$$v_{sp}\,(wt) = v_{spY}\,(wt) + v_{sp\Delta}\,(wt) \tag{31}$$

The advantage of the shadow projection is that there is no need to know the integration limits of the instanteous DC voltage in each interval, that requeires the calculation of the maximum and minimum AC instanteous voltages at each interval.

C. 18-PULSES TRUs SERIES CONNECTION

The 18-pulse TRU with three independent secondaries is analysed, considering that the primary is in star connection,

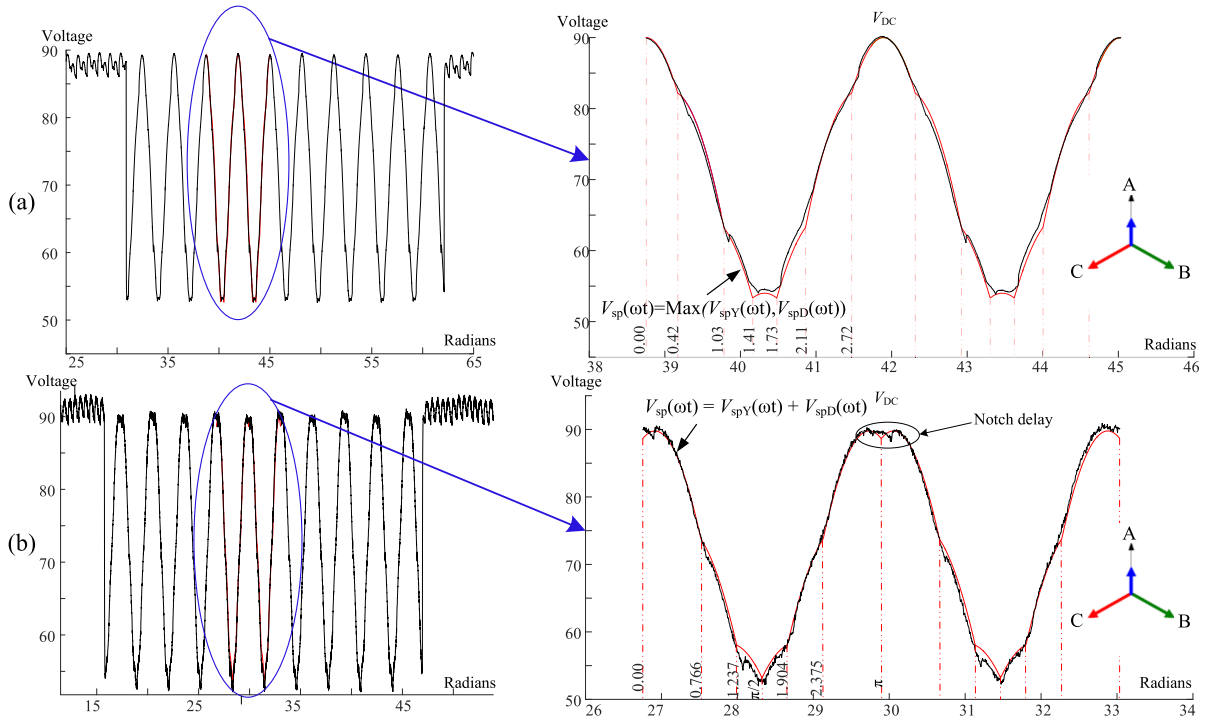

FIGURE 10. Experimental and the calculated values of the DC voltage for (a) parallel connection, (b) series connection.

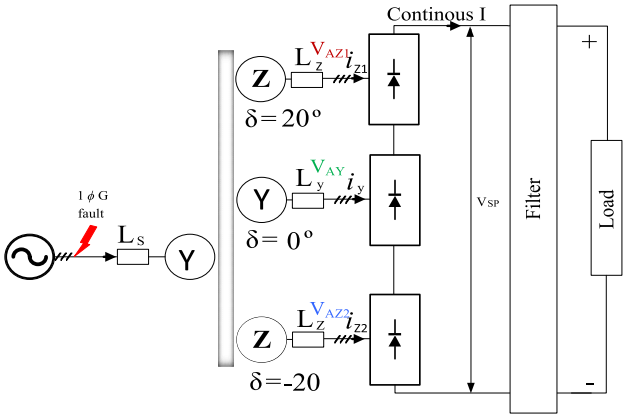

FIGURE 11. TRU 18-pulses Yz20°y0z-20° series connection with load.

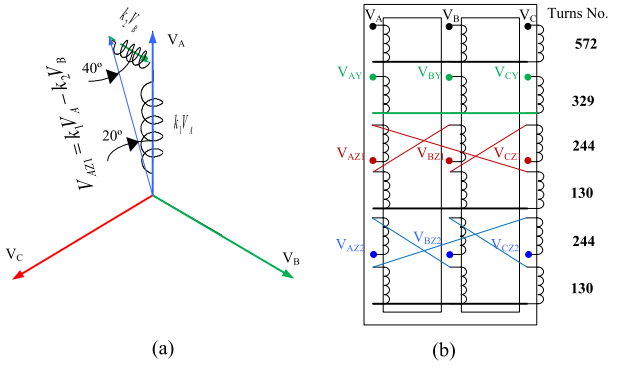

FIGURE 12. (a) Composition Voltage Vector V_{AZ1} from V_A and V_B direccions (b) transformer connection and turns number.

and the secondaries in, 20° zeta, 0° star and −20° zeta connections, respectively (Yz20°y0z-20°). The transformer winding connections are shown in Fig. 12(b), considering 0.699 V/turn. The shadow projection methodology is applied for a Type C sag (Fig. 14).

Knowing the primary voltages (second step in Fig. 13), the secondary voltages can be obtained considering the winding geometry (Fig. 12(a)), what can easily done in balanced system but is complex under supply voltage sags. The equations to calculate the secondary voltages are shown in the third step in Fig. 13 for the analysed transformer, where k_1 and k_2 are obtained through trigonometric relations using Fig 12(a):

$$|V_B|\, k_2 sen(40°) = |V_A|\, k_1 sen(20°) \tag{32}$$

$$\frac{|V_A|}{r_t} = |V_B|\, k_2 \cos(40°) + |V_A|\, k_1 cos(20°) \tag{33}$$

where r_t is the ratio transformar and is obtained using the following equation:

$$|V_A| = |V_B| = |V_C| \quad r_t = \frac{|V_A|}{|V_{AZ1}|} = \frac{|V_A|}{|V_{AY}|} \tag{34}$$

So, from the previous equation, k_1 and k_2 are calculated:

$$k_2 = k_1 \frac{sen(20°)}{sen(40°)}$$

$$k_1 = \frac{1}{r_t \left(\frac{sen(20°)}{sen(40°)} \cos(40°) + \cos(20°) \right)}$$

$$k_1 = 0.427, k_2 = 0.227 \tag{35}$$

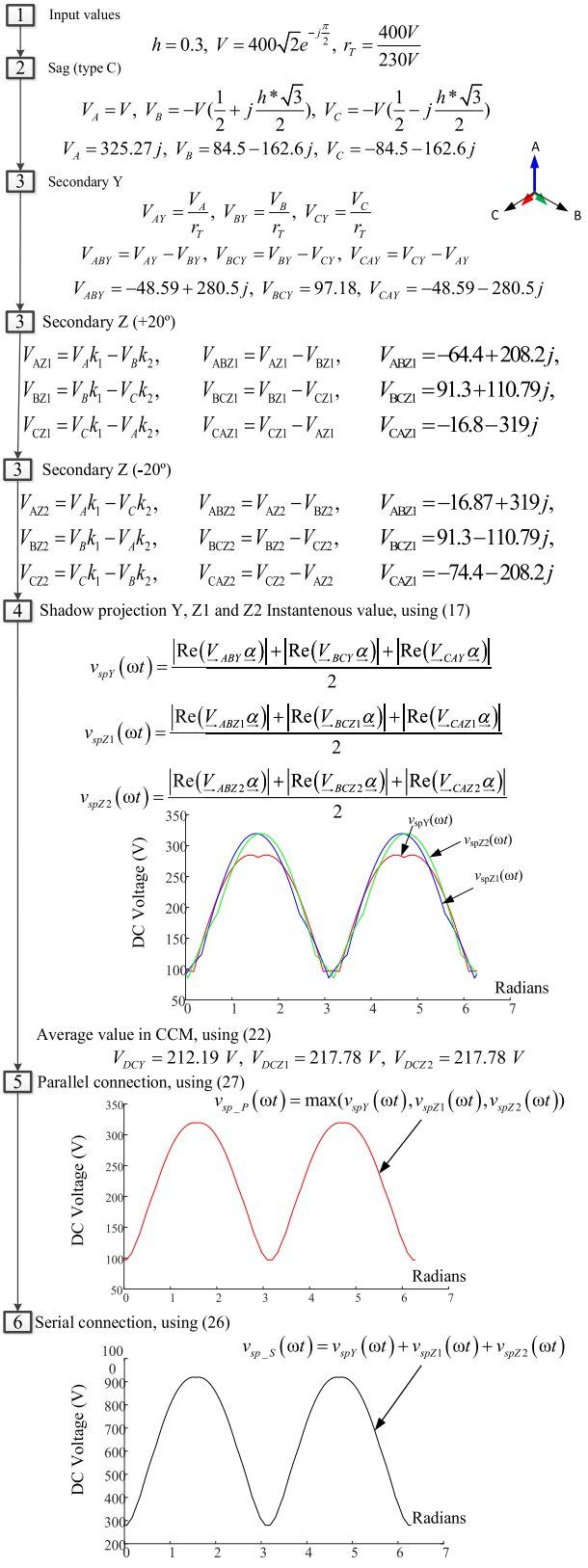

FIGURE 13. Flowchart of 18-pulse rectifier during unbalanced process to obtain the shadow projection voltage.

In the fourth step, the shadow projection voltage is calculated using (17) for every secondary. In the fifth step

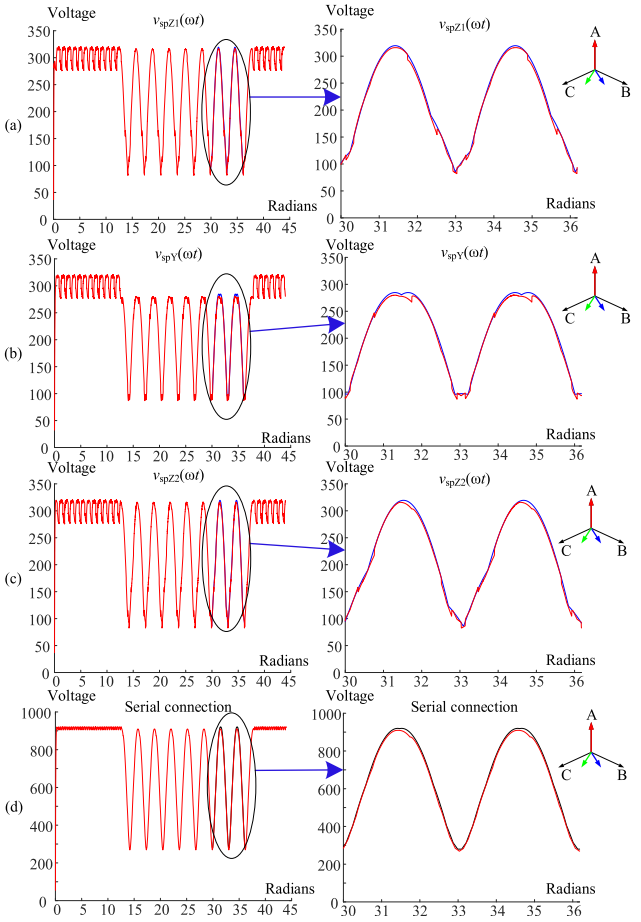

FIGURE 14. The secondery voltage for 18-pulses TRUs during a sag type C (a) Yz20°, (b) Yy0°, (c)Yz-20° (d) composed shadow projection voltage (step 6 in Fig. 13).

is composed with the parallel connection, in this case equation (27) is used.

In the sixth step, the voltage is calculated for serial connection using (26) and this connection is tested in the laboratory and the experimental signatures (red signal in Fig. 14) are superposed with the calculated values using the Shadow Projection methodology (blue signal in Fig. 14), and a good agreement between them can be observed. The average value shown in the fourth step in Fig. 13 are calculated using (22). While in this work a new methodology to calculate the instantaneous DC voltage for any TRU is presented, in the previous work presented in [30] only the average value was calculates using the convex hull method.

D. 36 PULSES PARALLEL CONNECTION TRUs AND USING INTERPHASE INDUCTORS

TRUs can be classified considering if the secondaries are isolated or not isolated. The TRUs analysed in sections B and C have isolated secondaries, while the TRU analysed in this section presents non-isolated secondaries. Non-isolated TRUs can increase the available power but serial connection is not possible and parallel connections only can be achieved

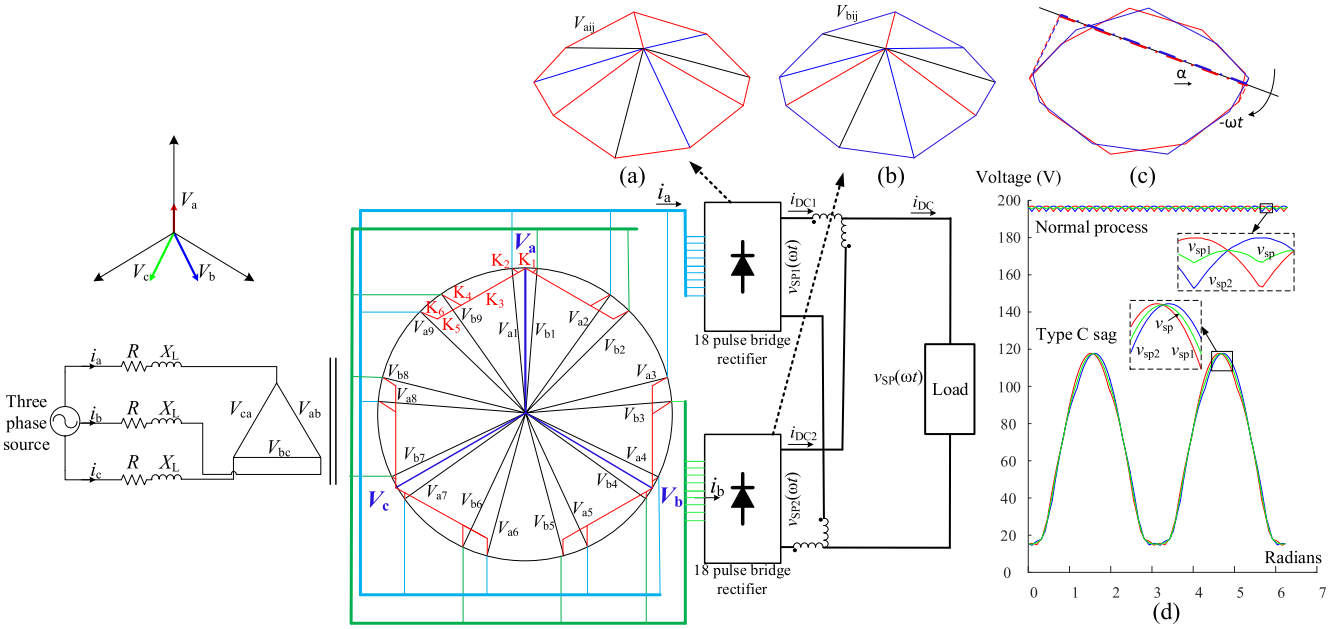

FIGURE 15. TRU 36 pulse with interphase inductors, in parallel connection with sag type C, $h = 0.3$ (a) First rectifier polygon, (b) Second rectifier polygon, (c) Both polygons with straight line and the projection on it, (d) normal voltage and voltage during Type C sag, for both rectifiers.

using interphase inductors that allow all the secondaries can operate at the same time.

The connection of 36-pulse TRU in parallel connection with interphase inductors is shown in Fig. 15. The transformer is connected to the two bridges with two nine-phase rectifiers each of them. In Fig. 15(a) and Fig. 15(b), the polygons of the two secondaries are shown for a Type C sag. Also, in Fig. 15(c), both polygons with a straight line and a shadow projection are represented. The voltage in normal conditions and during fault can be seen in Fig. 15(d). The shadow projection methodology is applied to create the output voltage signature for each rectifier during the Type C sag, and the flowchart for this unbalanced process to obtain the shadow projection voltage is presented in Fig. 16.

The supply phase voltages during Type C sag are defined according to Table 1 from [31], as follows:

$$V_A = V, \quad V_B = -V\left(\frac{1}{2} + j\frac{\sqrt{3}}{2} * h\right), \; V_C = -V\left(\frac{1}{2} - j\frac{\sqrt{3}}{2} * h\right) \tag{36}$$

The voltages of the fork transformer secondary are obtained using Table 4, which depends on the vector geometry, as seen in step 3 of Fig. 16. Then the nine sides of the polygon are constructed in step 4 of Fig. 16, and the shadow projection is obtained in this step. Each rectifier has its convex polygon, as shown in Fig. 15(a) and Fig. 15(b), and the sides of the polygons are calculated using (33).

$$V_{aij} = V_{ai} - V_{aj}, \quad V_{bij} = V_{bi} - V_{bj}, \quad j = i + 1 \tag{37}$$

The shadow projection is obtained by adding the nine sides of the polygon on the straight line and dividing them by two. In this case, the polygon is convex but irregular, as shown in Fig. 15 (a) and (b). If the two polygons are represented using the same center, as shown in Fig. 15(c), the polygon projections are closed to each other if the straight-line rotates with the polygons' center.

If the interphase inductors are used, both rectifiers work in parallel, and the $v_{SP}(\omega t)$ in step 7 is the average value of the two rectifiers' output voltage, using (28). The analysed configuration is only an example of the possible 36-pulse TRU configurations.

The Shadow Projection Methodology can be used for maintenance proposes, distinguishing between internal faults and grid faults. In the case of an internal fault, due

TABLE 4. Phase voltages of 36 pulses TRU.

Phases on Rectifier A	Phases on Rectifier B
$V_{a1} = V_a + k_1 V_c - k_2 V_b$	$V_{b1} = V_a + k_1 V_b - k_2 V_c$
$V_{a2} = V_a + k_3 V_b - k_4 V_c$	$V_{b2} = V_a + k_5 V_b - k_6 V_c$
$V_{a3} = V_b + k_5 V_a - k_6 V_c$	$V_{b3} = V_b + k_3 V_a - k_4 V_c$
$V_{a4} = V_b + k_1 V_a - k_2 V_c$	$V_{b4} = V_b + k_1 V_c - k_2 V_a$
$V_{a5} = V_b + k_3 V_c - k_4 V_a$	$V_{b5} = V_b + k_5 V_c - k_6 V_a$
$V_{a6} = V_c + k_5 V_b - k_6 V_a$	$V_{b6} = V_c + k_3 V_b - k_4 V_a$
$V_{a7} = V_c + k_1 V_b - k_2 V_a$	$V_{b7} = V_c + k_1 V_a - k_2 V_b$
$V_{a8} = V_c + k_3 V_a - k_4 V_b$	$V_{b8} = V_c + k_5 V_a - k_6 V_b$
$V_{a9} = V_a + k_5 V_c - k_6 V_b$	$V_{b9} = V_a + k_3 V_c - k_4 V_b$

where $k_1 = 0.05411$; $k_2 = 0.04651$; $k_3 = 0.512$; $k_4 = 0.1503$; $k_5 = 0.7011$; $k_6 = 0.1153$;

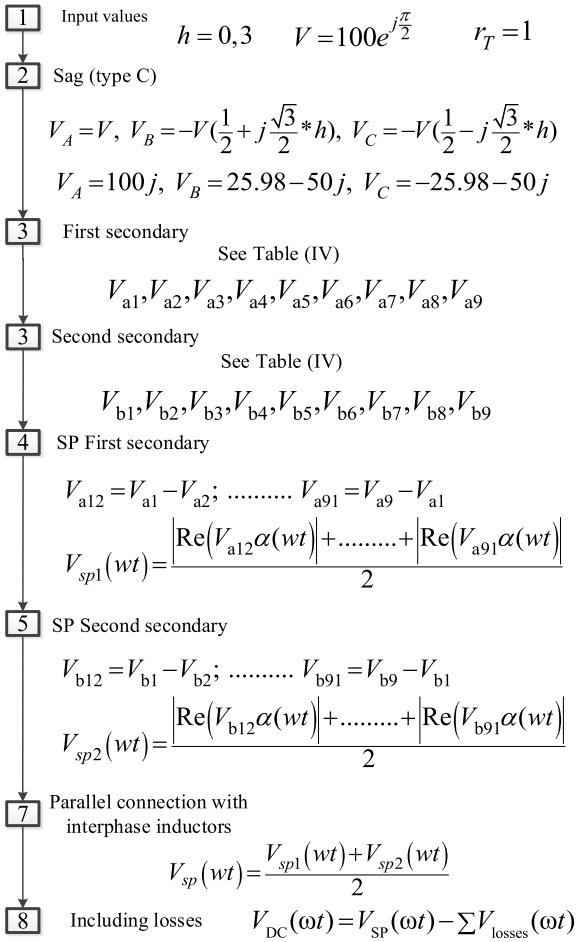

FIGURE 16. Flowchart of 36 pulse rectifier during unbalanced process to obtain the shadow projection voltage, with interphase inductors.

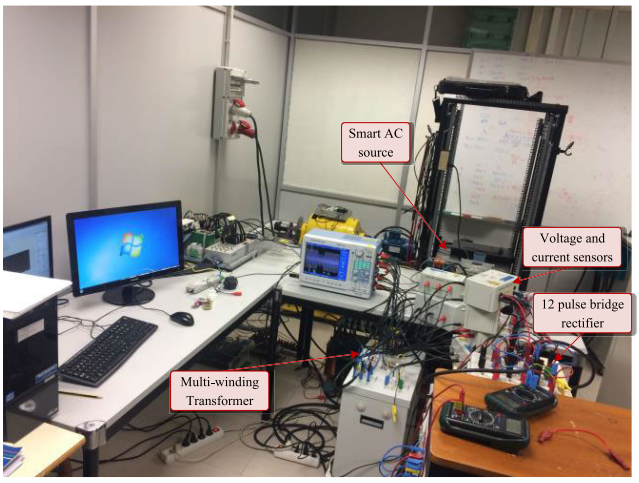

FIGURE 17. Experimental setup.

to transformer short-circuits or open-circuit diode of the rectifier, a not convex polygon is obtained.

V. EXPERIMENTAL SETUP

The experimental setup is shown in Fig. 17. The supply voltage sags were obtained using a Pacific Power Source Smart^{TM}, 4.5 kVA. Each uncontrolled bridge rectifiers consist of six SimicronTM ACKKD46/16 diodes.

The 12-pulse TRU was obtained using a power transformer 400/230/230 V and 4 kVA with Dy11d0 connection and two uncontrolled bridge rectifiers. The filter consists of a 9.8 mH inductor and a 12 μF capacitor, and the load is a 42 Ω resistor.

The 18-pulse TRUS was implemented using a multi-winding transformer 400/230/230/230 V and 2.4 kVA, with connection Yz20°y0°z-20°. The filter consists of 1 mH inductor, and the load is a 108 Ω resistor. The signals were recorded using the YOKOGAWATM DL850 scope.

VI. CONCLUSION

A new methodology is presented to calculate the instantaneous and average DC voltage for any TRU in balanced and unbalanced conditions. The shadow projection methodology allows to easily and quickly calculate the instantaneous and average DC voltage without determining the diode conduction intervals, only with the projection of the convex voltage polygons on a straight line. This methodology requires less compute power than other known methods. The main advantage over other methods is that the DC voltage signature can be accurately calculated for balanced and unbalanced conditions with any number of phases, which can be directly applied to any TRU.

The shadow projection methodology always presents a convex polygon during voltage sag and unbalanced process and it can be used to identify internal TRUs malfunctions; then, it can be used as a tool for maintenance in real time combined with Artificial Intelligence techniques.

REFERENCES

[1] S. Sau and B. G. Fernandes, "Modular multilevel converter based variable speed drive with reduced capacitor ripple voltage," *IEEE Trans. Ind. Electron.*, vol. 66, no. 5, pp. 3412–3421, May 2019.
[2] D. Zhang, H. Lin, Q. Zhang, S. Kang, and Z. Lu, "Analysis, design, and implementation of a single-stage multipulse flexible-topology thyristor rectifier for battery charging in electric vehicles," *IEEE Trans. Energy Convers.*, vol. 34, no. 1, pp. 47–57, Mar. 2019, doi: 10.1109/TEC.2018.2856905.
[3] E. I. Pool-Mazun, J. J. Sandoval, P. N. Enjeti, and I. J. Pitel, "An integrated solid-state transformer with high-frequency isolation for EV fast-charging applications," *IEEE J. Emerg. Sel. Topics Ind. Electron.*, vol. 1, no. 1, pp. 46–56, Jul. 2020, doi: 10.1109/jestie.2020.3003355.
[4] *IEEE Recommended Practices and Requirements for Harmonic Control in Electrical Power Systems*, IEEE Standard 519-1992, 1992.
[5] B. Wu, *High-Power Converters and AC Drives*, 2nd ed. Hoboken, NJ, USA: IEEE Press, 2006.
[6] H. Liu, F. Bu, W. Huang, L. Liu, Y. Hu, M. Degano, and C. Gerada, "Control strategy for five-phase dual-stator winding induction starter/generator system," *IEEE Trans. Ind. Electron.*, vol. 67, no. 4, pp. 2607–2617, Apr. 2020, doi: 10.1109/TIE.2019.2912767.
[7] P. P. Saravana, R. Kalpana, K. S. Chethana, and B. Singh, "A 36-pulse AC-DC converter with DC-side tapped interphase bridge rectifier for power quality improvement," *IEEE Trans. Ind. Appl.*, vol. 57, no. 1, pp. 549–558, Jan. 2021, doi: 10.1109/tia.2020.3028341.
[8] P. S. Prakash, R. Kalpana, and B. Singh, "Inclusive design and development of front-end multiphase rectifier with reduced magnetic rating and improved efficiency," *IEEE J. Emerg. Sel. Topics Power Electron.*, vol. 8, no. 3, pp. 2989–3000, Sep. 2020, doi: 10.1109/JESTPE.2019.2949138.

[9] T. H. Nguyen, D.-C. Lee, and C.-K. Kim, "A series-connected topology of a diode rectifier and a voltage-source converter for an HVDC transmission system," *IEEE Trans. Power Electron.*, vol. 29, no. 4, pp. 1579–1584, Apr. 2014, doi: 10.1109/TPEL.2013.2283368.
[10] J. Chen, Y. Shen, J. Chen, H. Bai, C. Gong, and F. Wang, "Evaluation on the autoconfigured multipulse AC/DC rectifiers and their application in more electric aircrafts," *IEEE Trans. Transport. Electrific.*, vol. 6, no. 4, pp. 1721–1739, Dec. 2020, doi: 10.1109/TTE.2020.2983858.
[11] A. Chaturvedi, D. Masand, S. Gupta, S. Tiwari, and M. Jain, "Comparative analysis of three phase AC-DC controlled multi pulse converter," in *Proc. IEEE Students Conf. Electr., Electron. Comput. Sci. (SCEECS)*, Mar. 2012, pp. 18–21, doi: 10.1109/SCEECS.2012.6184805.
[12] S. Khan, X. Zhang, M. Saad, H. Ali, B. M. Khan, and H. Zaman, "Comparative analysis of 18-pulse autotransformer rectifier unit topologies with intrinsic harmonic current cancellation," *Energies*, vol. 11, no. 6, p. 1347, May 2018, doi: 10.3390/en11061347.
[13] B. Singh and S. Gairola, "A 28-pulse AC–DC converter for line current harmonic reduction," *IET Electr. Power Appl.*, vol. 1, pp. 287–295, Jun. 2008, doi: 10.1049/iet-pel:20070239.
[14] B. Singh and S. Gairola, "Pulse doubling in 18-pulse AC-DC converters," in *Proc. 7th Int. Conf. Power Electron. Drive Syst.*, Nov. 2007, pp. 533–539.
[15] B. Singh, S. Gairola, B. N. Singh, A. Chandra, and K. Al-Haddad, "Multipulse AC-DC converters for improving power quality: A review," *IEEE Trans. Power Electron.*, vol. 23, no. 1, pp. 260–281, Jan. 2008, doi: 10.1109/TPEL.2007.911880.
[16] A. K. Singh, G. K. Singh, and R. Mitra, "Impact of source voltage unbalance on AC-DC rectifier performance," in *Proc. 2nd Int. Conf. Power Electron. Syst. Appl.*, Nov. 2006, pp. 96–101.
[17] B. Singh, V. Garg, and G. Bhuvaneswari, "A novel T-connected autotransformer-based 18-pulse AC-DC converter for harmonic mitigation in adjustable-speed induction-motor drives," *IEEE Trans. Ind. Electron.*, vol. 54, no. 5, pp. 2500–2511, Oct. 2007, doi: 10.1109/TIE.2007.900332.
[18] B. Singh, G. Bhuvaneswari, and V. Garg, "A novel polygon based 18-pulse AC-DC converter for vector controlled induction motor drives," *IEEE Trans. Power Electron.*, vol. 22, no. 2, pp. 488–497, Mar. 2007.
[19] S. Choi, P. N. Enjeti, and I. J. Pitel, "Polyphase transformer arrangements with reduced kVA capacities for harmonic current reduction in rectifier-type utility interface," *IEEE Trans. Power Electron.*, vol. 11, no. 5, pp. 680–690, Sep. 1996, doi: 10.1109/63.535400.
[20] Y. Zhang, J. Xia, X. Zhang, Z. Chen, B. Li, Q. Luo, and Y. He, "Modeling and prediction of the reliability analysis of an 18-pulse rectifier power supply for aircraft based applications," *IEEE Access*, vol. 8, pp. 47063–47071, 2020, doi: 10.1109/ACCESS.2020.2977197.
[21] J. S. Perisé, M. Bakkar, and S. B. Rodríguez, "Open-circuit fault diagnosis and maintenance in multi-pulse parallel and series TRU topologies," *IEEE Trans. Power Electron.*, vol. 35, no. 10, pp. 10906–10916, Oct. 2020, doi: 10.1109/TPEL.2020.2976895.
[22] M. H. Rashid, *Power Electronics: Circuits, Devices and Applications*, 3rd ed. Upper Saddle River, NJ, USA: Prentice-Hall, 2004.
[23] S.-G. Jeong and J.-Y. Choi, "Line current characteristics of three-phase uncontrolled rectifiers under line voltage unbalance condition," *IEEE Trans. Power Electron.*, vol. 17, no. 6, pp. 935–945, Nov. 2002, doi: 10.1109/TPEL.2002.805580.
[24] Z. Fang, T. Cai, S. Duan, C. Chen, and C. Ren, "Performance analysis and capacitor design of three-phase uncontrolled rectifier in slightly unbalanced grid," *IET Power Electron.*, vol. 8, no. 8, pp. 1429–1439, Aug. 2015, doi: 10.1049/iet-pel.2014.0421.
[25] M. Chen, Z. Qian, and X. Yuan, "Frequency-domain analysis of uncontrolled rectifiers," in *Proc. 19th Annu. IEEE Appl. Power Electron. Conf. Expo. (APEC)*, Feb. 2004, pp. 804–809, doi: 10.1109/APEC.2004.1295915.
[26] J. G. Mayordomo, L. F. Beites, X. Yang, and W. Xu, "A detailed procedure for harmonic analysis of three-phase diode rectifiers under discontinuous conduction mode and nonideal conditions," *IEEE Trans. Power Del.*, vol. 33, no. 2, pp. 741–751, Apr. 2018, doi: 10.1109/TPWRD.2017.2748384.
[27] M. Daryabak, S. Filizadeh, J. Jatskevich, A. Davoudi, M. Saeedifard, V. K. Sood, J. A. Martinez, D. Aliprantis, J. Cano, and A. Mehrizi-Sani, "Modeling of LCC-HVDC systems using dynamic phasors," *IEEE Trans. Power Del.*, vol. 29, no. 4, pp. 1989–1998, Aug. 2014, doi: 10.1109/TPWRD.2014.2308431.
[28] T. Yang, S. Bozhko, and G. Asher, "Functional modeling of symmetrical multipulse autotransformer rectifier units for aerospace applications," *IEEE Trans. Power Electron.*, vol. 30, no. 9, pp. 4704–4713, Sep. 2015, doi: 10.1109/TPEL.2014.2364682.
[29] D. Yuan, S. Wang, and Y. Liu, "Dynamic phasor modeling of various multipulse rectifiers and a VSI fed by 18-pulse asymmetrical autotransformer rectifier unit for fast transient analysis," *IEEE Access*, vol. 8, pp. 43145–43155, 2020, doi: 10.1109/ACCESS.2020.2977270.
[30] J. Saura, J. J. Mesas, and L. Sainz, "Average value of the DC-link output voltage in multi-phase uncontrolled bridge rectifiers under supply voltage balance and unbalance conditions," *Electr. Eng.*, vol. 103, no. 6, pp. 3097–3109, Dec. 2021, doi: 10.1007/s00202-021-01296-4.
[31] L. Guasch, F. Córcoles, and J. Pedra, "Effects of symmetrical and unsymmetrical voltage sags on induction machines," *IEEE Trans. Power Del.*, vol. 19, no. 2, pp. 774–782, Apr. 2004, doi: 10.1109/TPWRD.2004.825258.

JAUME SAURA-PERISE received the B.Sc. and M.Sc. degrees from the Polytechnic University of Catalonia, Barcelona, Spain, in 1986 and 1998, respectively. He worked at Aguas Ter Llobregat, at the Abrera drinking water treatment plant. Currently, he is a Professor with the Department of Electrical Engineering, Polytechnic University of Catalonia. He has three patents, such as the first was in 1991 about hexa-phase rectification, and two recent ones, about floatage control of a submersible vehicle. His research interests include power system quality, inverter control during faults, and fault diagnosis in electronic converters.

MOSTAFA BAKKAR received the B.Sc. degree in mechatronics engineering from the Alexandria Higher Institute of Engineering and Technology, Alexandria, Egypt, in 2008, and the M.Sc. degree in electrical and control engineering from Arab Academy for Science, Technology and Maritime Transport, Alexandria, in 2014. He is currently pursuing the Ph.D. degree with the Department of Electrical Engineering, Universitat Politècnica de Catalunya, Barcelona, Spain. His research interests include fault diagnosis, power system protection, artificial intelligence applications in power systems, smart grids, distributed power generation, and renewable energy systems.

SANTIAGO BOGARRA was born in Gavá, Spain, in May 1966. He received the Ph.D. degree in electrical engineering from the Polytechnic University of Catalonia, Barcelona, Spain, in 2002.

Currently, he is an Associate Professor of electrical engineering at the Polytechnic University of Catalonia, where he has been since 1997. He has published more than 40 conference and journal papers. His current research interests include electric aircraft and distributed generators connected to distributed power systems, further main areas of research are lightning protection and power system quality.